UNSTEADY FREE CONVECTION FROM A SPHERE IN A POROUS MEDIUM WITH VARIABLE SURFACE TEMPERATURE

A. Baradaran Rahimi, Taleb Jalali
Faculty of Engineering, Ferdowsi University of Mashhad, Mashhad, Iran.
rahimiab@yahoo.com

(Received:December 31, 2004)

Abstract In this paper a transient free convection flow around a sphere with variable surface temperature and embedded in a porous medium has been considered. The temperature of the sphere is suddenly raised and subsequently maintained at values that varies with position on surface. The method of asymptotic expansions is applied for small Rayleigh numbers and then a finite-difference scheme is used to solve the problem numerically for finite values of Rayleigh numbers. Transient and steady-state flow and temperature patterns around the sphere are discussed in details and a comparison between numerical and analytical results has been presented.

Keywords Transient, Rayleigh, Free convection, Sphere, Porous medium, Local Nusselt number

چکیده در این مقاله جابجایی آزاد گذرا در اطراف یک کره با درجه حرارت سطح متغیر که در داخل یک محیط متخلخل قرار گرفته مورد بررسی قرار می گیرد. درجه حرارت سطح این کره دفعتاً افزایش داده شده و متعاقبا در مقادیر درجه حرارتی نگه داشته می شود که با موقعیت سطح کره تغییر می کند. روش بسط مجانبی برای اعداد رایلی کوچک به کار گرفته شده و سپس برای مقادیر معین دیگری از این عدد، مسئله با استفاده از تکنیک های تفاضل محدود به صورت محاسباتی حل می شود. الگوهای جریان و درجه حرارت حالت پایدار و گذار در اطراف کره به صورت مفصل بحث شده و مقایسه ای بین حل عددی و نتایج تحلیلی ارائه می شود.

1. INTRODUCTION

Studies on natural convection around a sphere in fluid-saturated porous media are of interest in many engineering processes, such as thermal insulation systems, nuclear waste management, the storage of grain, in petroleum reservoirs and catalytic reactors. Yamamoto [1] was the first to consider the problem of steady natural convection around an isothermal sphere in porous medium. He obtained asymptotic solutions for small Rayleigh numbers. Subsequently, Merkin [2], Cheng [3], Nakayama and Koyama [4], and Pop and Ingham [5] considered high Rayleigh number (Ra) steady natural convection around a sphere with both an isothermal and non-isothermal surface. Sano and Okihara [6] and Sano [7] have studied the transient natural convection from a sphere in a porous medium using asymptotic solutions in terms of small Ra. Nguyen and Paik [8] have investigated the unsteady mixed convection from a sphere in a porous medium saturated with water numerically using a Chebyshev-Legeure spectral method. Yan et al. [9] performed a numerical study of unsteady free convection from a sphere embedded in a fluid-saturated porous medium when its surface is impulsively changing to a constant temperature or constant heat flux. Other studies about heat convection on a sphere with constant temperature have been done by Nazar and Pop [10], Kucaba-Pietal [11], and Alassar, badr and Marromatis [12]. All works on natural convection around a sphere in porous media, except [4] and [8], have been conducted only for constant temperature or constant heat flux on its surface. In this paper, we consider the problem of unsteady convection around a sphere in a porous medium when the temperature of its surface is changing with position. This situation is specially encountered when nuclear wastes, for example, are burried in earth. Initially the temperature of the surface is at a certain value and then it suddenly changes with location on the surface. First, we use perturbation analysis at small Rayleigh numbers. Then, by using a finite-difference method, the problem is solved numerically for finite values of Rayleigh numbers. The results obtained by perturbation analysis are compared with those obtained by numerical method for small Rayleigh numbers. For higher Rayleigh numbers, the results obtained by numerical methods are compared with those obtained by Yan et.al. [9] for constant surface temperature.

2. GOVERNING EQUATIONS

Consider a sphere of radius r_0 immersed in a fluid-saturated porous medium which is at a constant temperature. Suppose initially, that the sphere is in the same temperature as the porous medium and at time τ' it is suddenly heated and subsequently its surface temperature changes with position.

A spherical polar coordinate system (r',θ,ϕ) with the origin at the center of the sphere is chosen with $\theta = 0$ vertically upwards, as shown in Figure 1.

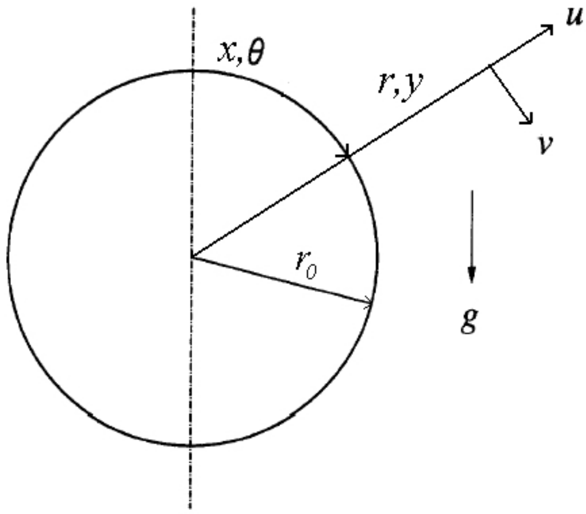

Figure 1. Polar coordinate system

Both the flow and temperature are assumed to be axially symmetric and hence independent of the azimuthal coordinate ϕ. The fluid motion is described by radial and transversal velocity component (u',v') in a plane through the axis of symmetry. The velocity component are expressed in terms of a dimensionless stream function $\psi(r,\theta)$ as,

$$u = \frac{1}{r^2 \sin\theta}\frac{\partial\psi}{\partial\theta} \qquad v = -\frac{1}{r\sin\theta}\frac{\partial\psi}{\partial r} \qquad (1)$$

If the physical properties of the fluid are assumed constant and the Darcy-Boussinesq approximation holds, then the non-dimensional governing equations in terms of the stream function ψ and temperature T can be written as

$$\frac{1}{r^2}\frac{\partial}{\partial\theta}\left(\frac{1}{\sin\theta}\frac{\partial\psi}{\partial\theta}\right)+\frac{1}{\sin\theta}\frac{\partial^2\psi}{\partial r^2} = \cos\theta\frac{\partial T}{\partial\theta}+r\sin\theta\frac{\partial T}{\partial r} \quad (2)$$

$$\frac{\partial T}{\partial\tau}+\frac{Ra}{r^2\sin\theta}\left(\frac{\partial T}{\partial r}\frac{\partial\psi}{\partial\theta}-\frac{\partial\psi}{\partial r}\frac{\partial T}{\partial\theta}\right) = \frac{1}{r^2}\frac{\partial}{\partial r}\left(r^2\frac{\partial T}{\partial r}\right)+\frac{1}{r^2\sin\theta}\frac{\partial}{\partial\theta}\left(\sin\theta\frac{\partial T}{\partial\theta}\right) \quad (3)$$

The dimensionless variables are defined as,

$$T=\frac{T'-T_\infty}{T_w-T_\infty},\quad r=\frac{r'}{r_0},\quad \tau=\frac{\alpha_m\tau'}{r_0^2},$$
$$u=\frac{u'}{U_r},\quad v=\frac{v'}{U_r}$$
$$U_r=\frac{Kg\beta(T_w-T_\infty)}{\upsilon},\quad Ra=\frac{Kg\beta(T_w-T_\infty)r_0}{\nu\alpha_m},$$
$$\psi=\frac{\psi'}{U_r r_0^2} \quad (4)$$

where K is the permeability of the thermal porous medium, β the coefficient of thermal expansion, ν the kinematic viscosity of the fluid, g the acceleration due to gravity, U_r the characteristic velocity, Ra the Rayleigh number and α_m the effective thermal diffusivity of the fluid-saturated porous medium .

Since the flow experiences larger gradients near the surface of the sphere, we introduce the following transformation to be used in numerical method,

$$r=\frac{\alpha}{1-x}-\alpha+1 \quad (5)$$

where α is a constant which, to some extent, can be used to control the mesh density when we set up the finite-difference scheme. Equations (2) and (3) in terms of the new variable (x,θ), become

$$\nabla^2\psi=\frac{1+(\alpha-1)x}{(1-x)}\sin\theta\times \left\{\sin\theta\frac{(1-x)^2}{\alpha}\frac{\partial T}{\partial x}+\frac{(1-x)\cos\theta}{[1+(\alpha-1)x]}\frac{\partial T}{\partial\theta}\right\} \quad (6)$$

$$\frac{\partial T}{\partial\tau}+\frac{Ra}{\sin\theta}\frac{(1-x)^4}{\alpha[1+(\alpha-1)x]^2}\times\left(\frac{\partial T}{\partial x}\frac{\partial\psi}{\partial\theta}-\frac{\partial\psi}{\partial x}\frac{\partial T}{\partial\theta}\right)= +\frac{2(1-x)}{[1+(\alpha-1)x]}\times\left\{\frac{(1-x)^2}{\alpha}\frac{\partial T}{\partial x}+\frac{(1-x)}{[1+(\alpha-1)x]}\cos\theta\frac{\partial T}{\partial\theta}\right\} \quad (7)$$

$$\nabla^2=\frac{(1-x)^4}{\alpha^2}\frac{\partial^2}{\partial x^2}-\frac{2(1-x)^3}{\alpha^2}\frac{\partial}{\partial x}+\frac{(1-x)^2}{[1+(\alpha-1)x]^2}\left(\frac{\partial^2}{\partial\theta^2}-\cot\theta\frac{\partial}{\partial\theta}\right) \quad (8)$$

At initial instant, $t\le 0$, we have

$$\psi=0, T=0 \quad , \quad 0\le x\le 1, \quad 0\le\theta\le\pi \quad (9a)$$

For t > 0, we have

$$\psi=0, T=f(\theta),\ x=0\ (r=1) \quad (9b)$$

$$\psi\to\frac{1}{2}r^2\sin^2\theta,\quad T\to 0,\quad x=1\ (r\to\infty) \quad (9c)$$

or for numerical method,

$$T=\frac{\partial\psi}{\partial x}=0,\quad x=1\ (r\to\infty) \quad (9d)$$

Finally, the symmetrical boundary conditions are:

$$\psi = \frac{\partial T}{\partial x} = 0, \; \theta = 0, \pi \; , \; 0 \le x \le 1 \tag{9e}$$

3. ASYMPTOTIC SOLUTION FOR SMALL RA NUMBERS

We shall now proceed to obtain asymptotic solutions of Equations (2) and (3) for small Ra using the method of matched asymptotic expansions. First, we solve these equations for steady-state condition and then we obtain solution of the transient condition .

3-1. Steady-state solution

We now assume that the Rayleigh number Ra is small and that the solutions may be expanded as,

$$\psi = \psi_0(r,\theta) + Ra\,\psi_1(r,\theta) + Ra^2\psi_2(r,\theta) + ... \tag{10}$$

$$T = T_0(r,\theta) + Ra T_1(r,\theta) + Ra^2 T_2(r,\theta) + ... \tag{11}$$

The equations for ψ_i and T_i with $i = 0,1,2,...$ can be found by substituting these expansions into (2) and (3) and collecting the terms containing the same power of Ra. The equation for T_0 is the pure heat conduction, and is as follows,

$$\frac{1}{r^2}\frac{\partial}{\partial r}\left(r^2\frac{\partial T_0}{\partial r}\right) + \frac{1}{r^2 \sin\theta}\frac{\partial}{\partial \theta}\left(\sin\theta\frac{\partial T_0}{\partial \theta}\right) = 0 \tag{12}$$

By setting $T_0(r,\theta) = F(r).G(\theta)$ and using boundary conditions (9b) and (9c) , we obtain

$$T_0(r,\theta) = \frac{a_n}{r^{n+1}} P_n(\cos\theta) \, , n = 0,1,2,\ldots \tag{13}$$

$$a_n = \frac{2n+1}{2}\int_0^{\pi}\left[f(\theta)P_n(\cos\theta)\sin\theta\right]d\theta \tag{14}$$

where $P_n(\cos\theta)$ is the Legendre function of order n .

By using a good approximation we can retain only two leading terms of Equation (13), therefore we have,

$$T_0(r,\theta) = \frac{a_0}{r} + \frac{a_1}{r^2}\cos\theta \tag{15}$$

The equation for ψ_0 is obtained from (2) in combination with T_0 obtained above and may be written as,

$$\frac{1}{r^2}\frac{\partial}{\partial\theta}\left(\frac{1}{\sin\theta}\frac{\partial\psi_0}{\partial\theta}\right) + \frac{1}{\sin\theta}\frac{\partial^2\psi_0}{\partial r^2} = -\frac{a_0}{r}\sin\theta - \frac{3a_1}{r^2}\sin\theta\cos\theta \tag{16}$$

By setting

$\psi_0(r,\theta) = a_0 f_0^{(0)}(r)\sin^2\theta + a_1 f_0^{(1)}(r)\sin^2\theta\cos\theta$

the required solution of (16) is found to be,

$$\psi_0(r,\theta) = \frac{a_0}{2}\left(r - \frac{1}{r}\right)\sin^2\theta + \frac{a_1}{2}\left(1 - \frac{1}{r^2}\right)\sin^2\theta\cos\theta \tag{17}$$

We can easily show that the effects of second terms in Equations (15) and (17) are negligible and so, we use only their first terms to obtain T_1, ψ_1, T_2, ψ_2. The method for determining $T_1, \psi_1, T_2, and\, \psi_2$ is straightforward, and we only show the final results below,

$$\begin{aligned} T(r,\theta) &= \frac{a_0}{r} + \frac{a_1}{r^2}\cos\theta \\ &+ Ra\left[a_0\left(\frac{1}{4r^3} - \frac{3}{4r^2} + \frac{1}{2r}\right)\cos\theta\right] \\ &+ Ra^2[a_0((-\frac{13}{180} + \frac{11}{240r^3}\ln r + \frac{3377}{30240r^3} \\ &- \frac{5}{72r^4} + \frac{27}{1120r^5} + (\frac{5}{48r} - \frac{5}{16r^2} + \frac{11}{80r^3}\ln r \\ &+ \frac{2537}{10080r^3} - \frac{5}{96r^4} + \frac{5}{224r^5})\cos 2\theta))] \end{aligned} \tag{18}$$

$$\psi(r,\theta)=\frac{a_0}{2}(r-\frac{1}{r})\sin^2\theta+\frac{a_1}{2}(1-\frac{1}{r^2})\sin^2\theta\cos\theta+$$
$$+Ra\left[a_0(-\frac{3}{8}+\frac{1}{6}r+\frac{1}{4r}-\frac{1}{24r^2})\sin^2\theta\cos\theta\right]$$
$$+Ra^2[a_0((-\frac{23r}{576}+\frac{13}{160r}\ln r+\frac{163}{25200r}+\frac{5}{228r^2}$$
$$+\frac{3}{224r^3}\ln r+\frac{541}{33600r^3})\sin^2\theta+$$
$$(\frac{5r}{192}-\frac{5}{48}+\frac{11}{160r}\ln r+\frac{461}{5040r}-\frac{5}{96r^2}+$$
$$\frac{5}{224r^3}\ln r+\frac{781}{20160r^3})\sin^2\theta\cos 2\theta)] \tag{19}$$

The local Nusselt number is defined as $Nu=-\frac{\partial T}{\partial r}|_{r=1}$, so from (18) one obtaines:

$$Nu=a_0+2a_1\cos\theta-Ra(.25a_0\cos\theta)+Ra^2(.0597a_0) \tag{20}$$

Also from (18), the average Nusselt number may be calculated as

$$\overline{Nu}=-\frac{1}{2}\int_0^{\pi}\frac{\partial T}{\partial r}|_{r=1}(\sin\theta)d\theta=a_0+\frac{269}{5040}Ra^2 \tag{21}$$

3-2) Transient solution

In the small-time domain, where $Ra=O(1)$, the solutions of Equations (2) and (3) are expanded as,

$$t=t_0(r,\theta,\tau)+Rat_1(r,\theta,\tau) \tag{22}$$

$$\psi=\psi_0(r,\theta,\tau)+Ra\psi_1(r,\theta,\tau) \tag{23}$$

respectively. These expansions are uniformly valid for $1\le r\le\infty$, since the temperature layer is confined to the inner region near the surface where $r=O(1)$ and the convective term is of minor importance compared to the conduction and unsteady terms. Inserting Equations (22) and (23) into Equations (2) and (3), we obtain the following equations for t_0,ψ_0,

$$\frac{\partial t_0}{\partial\tau}=\nabla^2 t_o \tag{24}$$

$$\frac{1}{r^2}\frac{\partial}{\partial\theta}(\frac{1}{\sin\theta}\frac{\partial\psi_0}{\partial\theta})+\frac{1}{\sin\theta}\frac{\partial^2\psi_0}{\partial r^2}$$
$$=\cos\theta\frac{\partial t_0}{\partial\theta}+r\sin\theta\frac{\partial t_0}{\partial r} \tag{25}$$

The solutions of Equations (24) and (25) satisfying the corresponding boundary and initial conditions may easily be obtained as,

$$t_0(r,\theta)=\frac{a_0}{r}erf(\eta)+\frac{a_1}{r^2}\cos\theta \tag{26}$$

$$\psi_0=a_0[\frac{1}{2}(r-\frac{1}{r}-\frac{2\tau}{r})erfc(\eta)$$
$$+\frac{1}{r}(2\sqrt{\frac{\tau}{\pi}}(1-e^{-\eta^2})-\frac{2\tau}{\pi}\eta e^{-\eta^2}+\tau)]\sin^2\theta \tag{27}$$

respectively, where,

$$\eta=\frac{r-1}{2\sqrt{\tau}} \tag{28}$$

We can show that these solutions approach the corresponding steady-state solutions as $\tau\to\infty$, suggesting that they are uniformly valid for $0\le\tau\le\infty$. We can also show, as described by Sano and Makizono [13], that the second terms in Equations (24) and (25), namely t_1 and ψ_1, do not approach their corresponding steady-state solutions. This suggests that Equation (24) and (25) are invalid for large τ. This is due to the fact that as τ increases the temperature layer diffuses into the outer region far from the sphere, where $r=o(Ra^{-1})$ and convection effects are not negligible even when $Ra\to 0$. This fact suggests that the temperature field (and therefore the velocity field) for large τ have a two-region structure in r, namely, a large-time inner region and a large-time outer region and that we must construct two expansions for ψ and t which are valid in these two large-time regions. A time variable appropriate for large τ is,

$$\tau^* = Ra^2 \tau \tag{29}$$

In the large-time inner region, where $r = O(1)$ and $\tau = o(Ra^{-2})$, the governing equations may be written as,

$$Ra^2 \frac{\partial t^*}{\partial \tau^*} + \frac{Ra}{r^2 \sin\theta}\left(\frac{\partial t^*}{\partial r}\frac{\partial \psi^*}{\partial \theta} - \frac{\partial \psi^*}{\partial r}\frac{\partial t^*}{\partial \theta}\right) = \nabla^2 t^* \tag{30}$$

$$\begin{aligned}&\frac{1}{r^2}\frac{\partial}{\partial\theta}\left(\frac{1}{\sin\theta}\frac{\partial\psi^*}{\partial\theta}\right) + \frac{1}{\sin\theta}\frac{\partial^2\psi^*}{\partial r^2}\\ &= \cos\theta\frac{\partial T^*}{\partial\theta} + r\sin\theta\frac{\partial t^*}{\partial r}\end{aligned} \tag{31}$$

where,

$$\begin{aligned}&t^*(r,\theta,\tau^*) = t(r,\theta,\tau),\\ &\psi^*(r,\theta,\tau^*) = \psi(r,\theta,\tau)\end{aligned} \tag{32}$$

Solutions of Equations (30) and (31) are assumed to be of the form (large-time inner expansions),

$$t^*(r,\theta,\tau^*) = t_0^*(r,\theta,\tau) + Ra\, t_1^*(r,\theta,\tau) \tag{33}$$

$$\psi^*(r,\theta,\tau^*) = \psi_0^*(r,\theta,\tau) + Ra\, \psi_1^*(r,\theta,\tau) \tag{34}$$

respectively. The following outer variables are introduced in the large-time outer region far from the sphere, where $r = o(Ra^{-1})$ and $\tau = o(Ra^{-2})$:

$$\rho = Ra\ r, \tag{35}$$

$$\begin{aligned}&T^*(\rho,\theta,\tau^*) = Ra^{-1} T^*(r,\theta,\tau^*),\\ &\Psi^*(\rho,\theta,\tau^*) = Ra^2 \psi^*(r,\theta,\tau^*)\end{aligned} \tag{36}$$

in terms of which the governing equations become,

$$\frac{\partial T^*}{\partial \tau^*} + \frac{1}{\rho^2 \sin\theta}\left(\frac{\partial T^*}{\partial \rho}\frac{\partial \Psi^*}{\partial \theta} - \frac{\partial \Psi^*}{\partial \rho}\frac{\partial T^*}{\partial \theta}\right) = \nabla_\rho^2 T^* \tag{37}$$

$$\begin{aligned}&\frac{1}{\rho^2}\frac{\partial}{\partial\theta}\left(\frac{1}{\sin\theta}\frac{\partial\Psi^*}{\partial\theta}\right) + \frac{1}{\sin\theta}\frac{\partial^2\Psi^*}{\partial \rho^2}\\ &= Ra\left(\cos\theta\frac{\partial T^*}{\partial\theta} + \rho\sin\theta\frac{\partial T^*}{\partial \rho}\right)\end{aligned} \tag{38}$$

where ∇_ρ^2 is the same operator as ∇^2, but with r replaced by ρ. The solutions of these equations are assumed to be of the form (large-time outer expansions),

$$T^*(r,\theta,\tau^*) = T_0^*(r,\theta,\tau) + Ra\, T_1^*(r,\theta,\tau) \tag{39}$$

$$\Psi^*(r,\theta,\tau^*) = \Psi_0^*(r,\theta,\tau) + Ra\, \Psi_1^*(r,\theta,\tau) \tag{40}$$

The boundary conditions on the surface are imposed on the inner expansions, Equations (33) and (34), and the one at infinity on the outer expansions, Equations (39) and (40). The matching conditions between the inner and outer expansions are,

$$\lim_{\rho\to 0} T^*(\rho,\theta,\tau^*) = \lim_{r\to\infty} Ra^{-1} t^*(r,\theta,\tau^*) \tag{41}$$

and

$$\lim_{\rho\to 0} \Psi^*(\rho,\theta,\tau^*) = \lim_{r\to\infty} Ra^{-2} \psi^*(r,\theta,\tau^*) \tag{42}$$

Furthermore, the expansion for T^* is required to satisfy the following matching condition with the small-time expansion, Equation (22),

$$\lim_{\tau^*\to 0} T^*(\rho,\theta,\tau^*) = 0 \tag{43}$$

This is because the thermal layer in the small-time region is confined to the inner region near the surface.
The solutions in the large-time region are obtained for $t_0^*, t_1^*, T_0^*, \psi_0^*, \psi_1^*, \Psi_0^*$ and Ψ_1^*. Since the procedure of obtaining these solutions is similar to

that described in Sano [14], only the final results are presented below,

$$t_0^* = \frac{a_0}{r} + \frac{a_1}{r^2}\cos\theta \tag{44}$$

$$t_1^* = a_0\left(\left(\frac{1}{r}-1\right)\left\{\frac{1}{\sqrt{\pi\tau^*}}e^{-(1/4)\tau^*} + \frac{1}{2}erf\left(\frac{1}{2}\sqrt{\tau^*}\right)\right\} + \left\{\frac{1}{2}+\frac{1}{2r}-\frac{3}{2r^2}+\frac{1}{2r^3}\right\}\cos\theta\right) \tag{45}$$

$$T_0^* = \frac{a_0}{2\rho}e^{(1/2)\rho\mu} \times\left\{e^{\rho/2}erfc\left(\frac{\rho}{2\sqrt{\tau^*}}+\frac{\sqrt{\tau^*}}{2}\right)+e^{-\rho/2}erfc\left(\frac{\rho}{2\sqrt{\tau^*}}-\frac{\sqrt{\tau^*}}{2}\right)\right\},\ \mu=\cos\theta \tag{46}$$

$$\psi_0^* = a_0\left\{\frac{1}{2}r^2-\frac{1}{2}r\right\}\sin^2\theta \tag{47}$$

$$\psi_1^* = a_0\left(\left\{b_1r^2+\left(\frac{b_0}{2}-b_1\right)\frac{1}{r}-\frac{b_0}{2}r\right\}\sin^2\theta + \left\{-\frac{3}{4}+\frac{1}{2r}+\frac{1}{6}r+\frac{1}{8}r^2-\frac{1}{24}r^2\right\}\cos\theta\sin^2\theta\right) \tag{48}$$

$$\Psi_0^* = \frac{1}{2}a_0\rho^2\sin^2\theta \tag{49}$$

$$\begin{aligned}\Psi_1^* = -\frac{2}{3}a_0\Big[&-\frac{3}{2}\mu-\frac{3}{4}(1-\mu)erf\left(\frac{\rho}{2\sqrt{\tau^*}}+\frac{\sqrt{\tau^*}}{2}\right)\\ &\times\left\{1-\exp\left(\frac{\rho}{2}(1+\mu)\right)\right\}+\frac{3}{4}(1+\mu)erf\left(\frac{\rho}{2\sqrt{\tau^*}}-\frac{\sqrt{\tau^*}}{2}\right)\\ &\times\left\{1-\exp\left(-\frac{\rho}{2}(1-\mu)\right)\right\}\rho^2\sin^2\theta-\frac{3}{2}\exp\left(\frac{\mu\rho}{2}\right)\\ &\times\left[\sinh\frac{\rho}{2}-\mu\cosh\frac{\rho}{2}\right]+\frac{3}{2}(\pi\tau^*)^{-1/2}\exp\left(-\frac{\rho^2}{4\tau^*}-\frac{\tau^*}{4}\right)\\ &\times\left[\exp\left(\frac{\mu\rho}{2}-\cosh\frac{\rho}{2}-\mu\sinh\frac{\rho}{2}\right)\right]\Big]\end{aligned} \tag{50}$$

where,

$$b_o = -\left\{\frac{1}{\sqrt{\pi\tau^*}}e^{-(1/4)\tau^*}+\frac{1}{2}erf\left(\frac{1}{2}\sqrt{\tau^*}\right)\right\} \tag{51}$$

$$b_1 = -\frac{1}{8} \times\left\{\left(\frac{4}{\tau^{*2}}+1\right)erf\left(\frac{1}{2}\sqrt{\tau^*}\right)+\frac{2}{\sqrt{\pi\tau^*}}\left(1-\frac{2}{\tau^*}\right)e^{-(1/4)\tau^*}\right\} \tag{52}$$

In order to complete the present analysis, it is desirable to obtain the second terms ψ_1 and t_1 in the small-time expansions, since the large-time inner solutions have been obtained up to the term of $O(Pe)$. Unfortunately, however, it is very difficult to obtain these terms so here we only show the asymptotic solutions for small τ instead, as obtained by Sano[14]. These results are,

$$t_1 = t_{1F}(r,\theta,\tau)+\left\{F_0(\eta)\tau+O(\tau^{3/2})\right\}\cos\theta \tag{53}$$

$$\psi_1 = \left\{\frac{-3}{\sqrt{\pi}}(e^{-\eta^2}-1)+\int_0^\eta F_0(\eta)d\eta\right\} \times(\sin^2\theta\cos\theta)\tau^{3/2}+O(\tau^{3/2}) \tag{54}$$

$$t_{1F} = \frac{a_0}{4} \times\left\{\begin{aligned}&3(r^{-2}-r^{-1})\exp(r-1+\tau)erfc(\eta+\tau^{1/2})\\&+(-r^{-3}-3r^{-2}+2)erfc\eta\end{aligned}\right\}\cos\theta \tag{55}$$

where

$$\begin{aligned}F_0(\eta) &= -2.951(Hh_2(\sqrt{2}\eta))\\ &+2.548Hh_2(\sqrt{2}\eta)\{2Hh_4(\sqrt{2}\eta)+2.828Hh_3(\sqrt{2}\eta)\\ &+(2\eta^2+1)Hh_2(\sqrt{2}\eta)+.943\eta^3+\sqrt{2}\eta\}\\ &+2.548(2\eta^2+1)\{-.5(Hh_2(\sqrt{2}\eta))^2+Hh_3(\sqrt{2}\eta)\}\end{aligned} \tag{56}$$

$$Hh_n(x) = \begin{cases} \int_0^\infty \frac{t^n}{n!} \exp\{-\frac{1}{2}(t+x)^2\} dt & n \geq 0 \\ (-1)^{n-1} (\frac{d}{dx})^{-n-1} \exp(-\frac{1}{2}x^2) & n < 0 \end{cases} \quad (57)$$

n is an integer number .

4. NUMERICAL SOLUTION

Equations (6) and (7) are now solved numerically using a finite-difference scheme subject to boundary conditions (9a)-(9e). We use central-difference and fully explicit schemes to Equations (6) and (7), respectively. The discretized stream equation and energy equation are solved by using a line by line TDMA (Tri Diagonal-Matrix Algorithm). In each iteration, first, Equation (6) is solved by using a point relaxation and in the iteration process for ψ, the most updated values for ψ and T on the adjacent lines are used. Then Equation (7) is solved and the same procedure is applied. The convergence criterion for iterations is chosen as follows,

$$\sum \left\{ \left| \psi^{(m)} - \psi^{(m-1)} \right| + \left| T^{(m)} - T^{(m-1)} \right| \right\} < \varepsilon \quad (58)$$

where ε is the prescribed tolerance and the summation takes place over all the mesh points. For the steady state solution, the above procedure is carried out until τ is sufficiently large so that the solutions for two successive time steps are almost identical.

5. RESULTS AND DISCUSSIONS

Analytical, as well as numerical results were obtained for unsteady free convection from a sphere with variable surface temperature in a porous medium for $0.1 \leq Ra \leq 50$. The mesh sizes and the value of the constant parameter α for the calculations presented in this paper vary with Rayleigh number and are shown in table 1.

Table 1. The magnitudes of parameters used in numerical solution

Ra	Δx	$\Delta\theta$	Δt	α	ε
.1-5	1/60	1/60	.01	1	10^{-5}
5-10	1/120	1/80	.01	1.5	10^{-5}
10-30	1/140	1/80	.05	3	10^{-5}
30-50	1/160	1/90	.05	5	10^{-5}

It is found that numerical results are more sensitive to the mesh sizes in *x*-direction than to that in the θ-direction. For small Rayleigh numbers, we compare results obtained by numerical methods with those obtained by analytical methods. Since there are no results for variable temperature in large Rayleigh numbers, we compare numerical results obtained in this work with those presented in [9] for constant temperature case. We have evaluated many functions for variation of temperature on surface of sphere and in this paper, for brevity the main results for function $T(s) = 1.0 + 0.1\cos\theta$ are shown.

Figure (2) shows the instantaneous streamlines for Ra=50 at time τ = 1, 15 and 50 for special case of constant surface temperature. These results compare very well with those obtained by Yan et.al. [9] which have been shown here following this figure scanned from this reference, (Fig. 2, page 898).

The instantaneous streamlines for Ra = 0.4 and 10 at time $\tau = 1$, 10, and 50 are shown in Figures (3) and (4) for surface temperature function $T(s) = 1.0 + 0.1\cos\theta$. As it is seen from the figures, fluid is entrained towards the hot sphere and an upward flow is generated along the sphere surface. In the early stages, the fluid motion is mainly confined to the vicinity of the sphere whilst

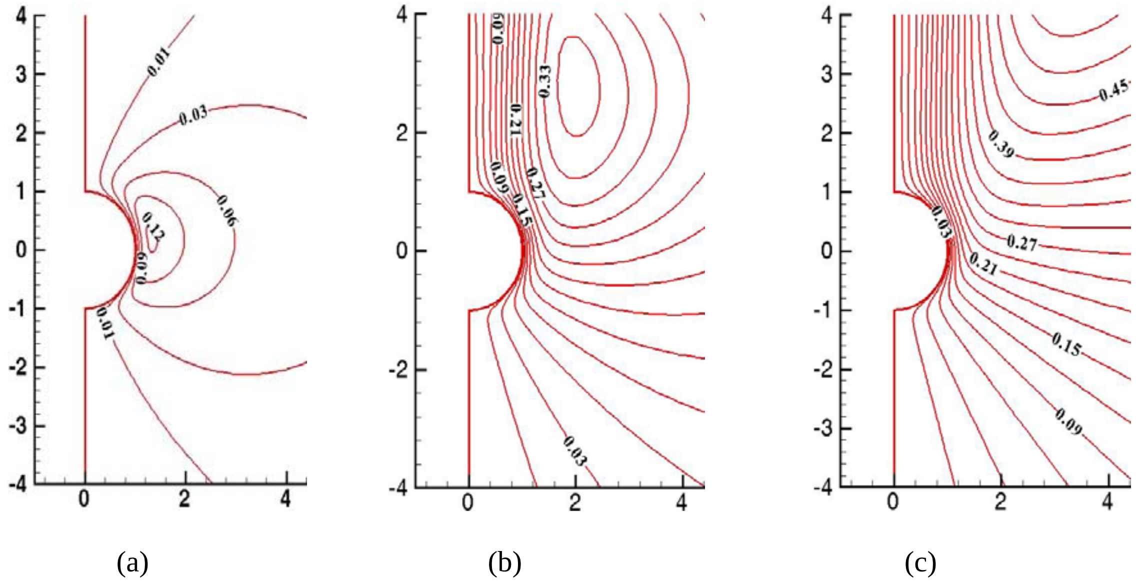

Figure 2. The instantaneous streamlines for Ra = 50 and constant temperature at different times :
(a) τ = 1 , (b) τ = 15 , (c) τ = 50

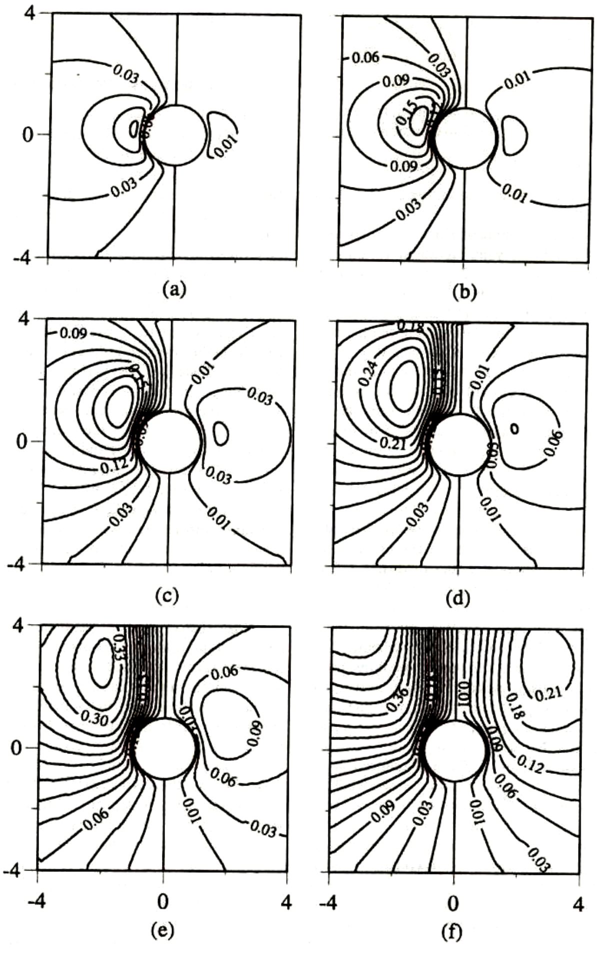

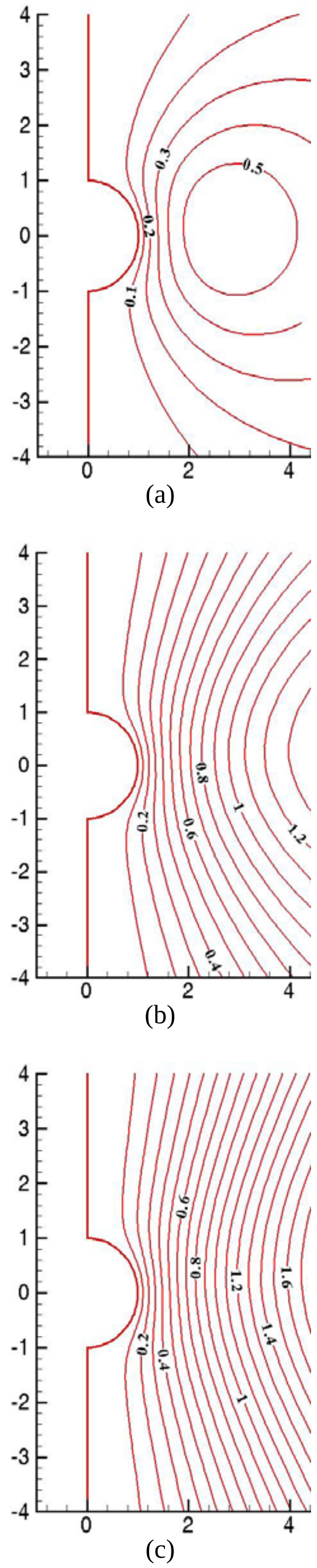

Figure 3. The instantaneous streamlines for Ra = .4 at different times : (a) τ = 1 , (b) τ = 10 , (c) τ = 50

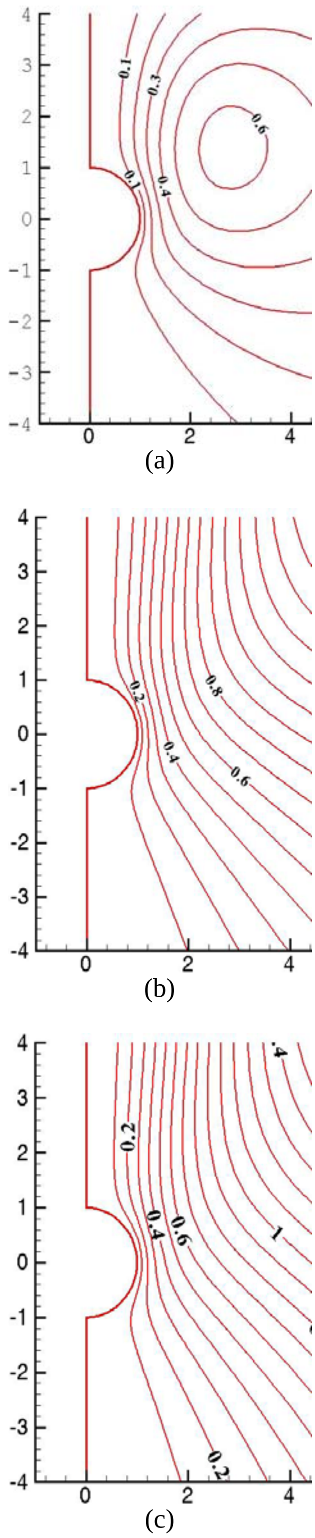

Figure4. The instantaneous streamlines for Ra = 10 at different times : (a) τ = 1 , (b) τ = 10 , (c) τ = 50

at later times, due to convection from sphere, the flow motion spreads outwards and upwards. It is also seen that a vortex ring surrounded by the main flow appears which surrounds the sphere. For small Ra numbers, because of weakness of convection effects, the streamlines are symmetrical with respect to plane $\theta = 90^o$ but as Ra number increases the core of this vortex ring moves up due to convection effect becoming stronger. From about $\tau = 10$, the flow pattern very close to sphere does not change very much but variation of streamlines with respect to time increases in far away distances from the sphere. Reaching steady state conditions may not become possible but the flow near the sphere will approach to steady state situation after a relatively long time.

The temperature contours for $Ra = 0.4$ and 10 at $\tau = 1, 10$ are depicted in Figures (5) and (6), respectively. For $Ra = 0.4$, the isothermal lines are nearly circular and as Ra increases convection effects become stronger and for $Ra = 10$ and at $\tau = 50$ a very clear cap of a plum is observed which moves upwards as the convection process continues. It is also noted that as Ra increases, the thermal boundary layer thickness decreases at the bottom of the sphere and increases at the top of it.

Figures (7) and (8) show the steady-state distribution of radial and tangential velocity for $Ra = 0.1$ and 0.4 for different values of θ which were obtained using numerical and analytical methods. As evident from these figures, there is a very good agreement between the two methods.

Figure (9) shows the unsteady distribution of radial velocity in terms of radial distance r for $Ra = 0.4$ and 10 at $\theta = 0$ and for various time values. It is seen that the value of radial velocity increases from zero to a maximum value on the surface of the sphere and then decreases to zero as this radial distance increases. Also, for a certain Ra number as τ increases, the value of radial velocity increases due to convection effects becoming stronger.

Figure (10) shows variation of radial velocity for $Ra = 1{,}10$ and $\tau = 10$ in terms θ. It is seen that for a certain Ra number as θ increases, the value of radial velocity decreases and near the plane $\theta = 90^0$ tends to zero. After this plane as θ increases, the value of radial velocity increases in opposite direction and this process continues until $\theta = 180^o$. This means that velocity has only radial component at $\theta = 0^0$ and 180^0, and only tangential component at $\theta = 90^0$. Also for $Ra = 10$ the value of radial velocity at $\theta = 0^0$ is greater than its corresponding value for $Ra = 1$ but at $\theta = 180^0$ this situation is reverse. To explain this, consider Figures (3) and (4). It is evident that because of upward movement of vortex ring for greater Ra numbers like $Ra = 10$ and at $\theta = 0^0$ the streamlines are very close to each other but at $\theta = 180^0$ the distance of the streamlines with respect to corresponding values for smaller Ra numbers are greater and this causes smaller radial velocities for greater Ra numbers.

Figure (11) shows the distribution of transient tangential velocity for $Ra = 0.4$ and 10 in different time values and at $\theta = 90^0$. As from the figures, the maximum value of tangential velocity is on the surface of the sphere and as the radial distance increases these maximum values tend to zero gradually. For greater Ra numbers like $Ra = 10$ and at the vicinity of the sphere at $\theta = 90^0$ the magnitude of tangential velocity is greater than the corresponding value for smaller Ra numbers like $Ra = 0.4$ but far away from the sphere these values are smaller for smaller Ra numbers. This is due to the fact that the center of the vortex ring moves upward with increasing Ra number but for small Ra numbers like $Ra = 0.4$ this center is approximately located on plane $\theta = 90^0$. Therefore for smaller Ra numbers the streamlines are closer to each other.

Figure (12) shows the variation of transient tangential velocity in terms of different values of θ for $Ra = 0.4{,}10$ at τ =1. It is observed that for $Ra = 10$ the values of tangential velocity close to the plane $\theta = 90^0$ and near the surface of the sphere are higher than the corresponding values for other angles, but outside this region the values of tangential velocities in plane $\theta = 30^0$ is greater than the corresponding values for other angles. It is also observed that for $Ra = 0.4$ the values of tangential velocities in plane $\theta = 90^0$ along the radial distance are greater than the corresponding

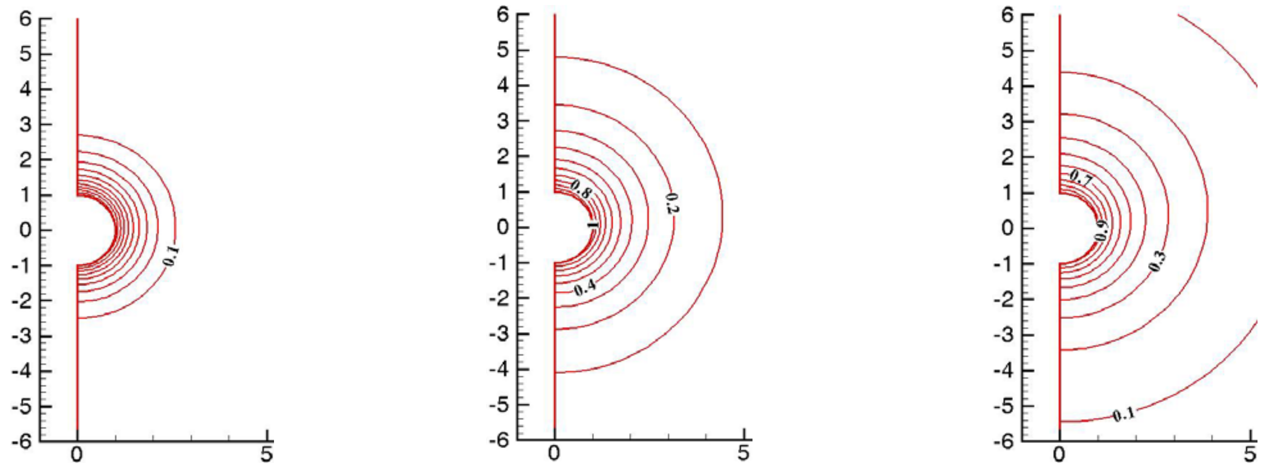

(a) (b) (c)

Figure 5. The instantaneous isotherm lines for Ra = .4 at different times : (a) τ = 1 , (b) τ = 10 , (c) τ = 50

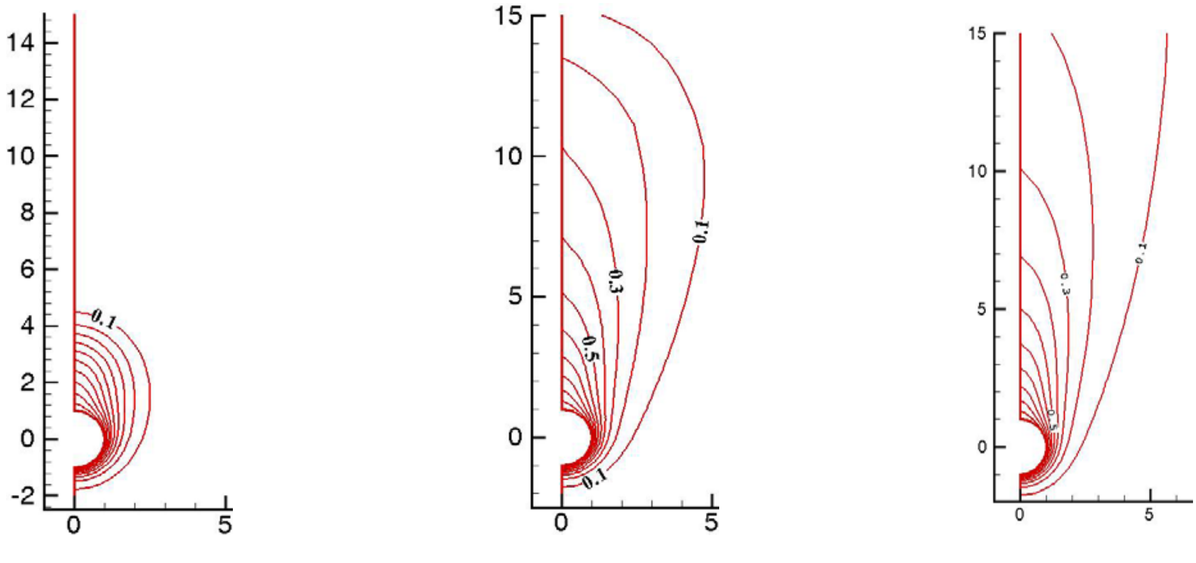

(a) (b) (c)

Figure 6. The instantaneous isotherm lines for Ra = 10 at different times : (a) τ = 1 , (b) τ = 10 , (c) τ = 50

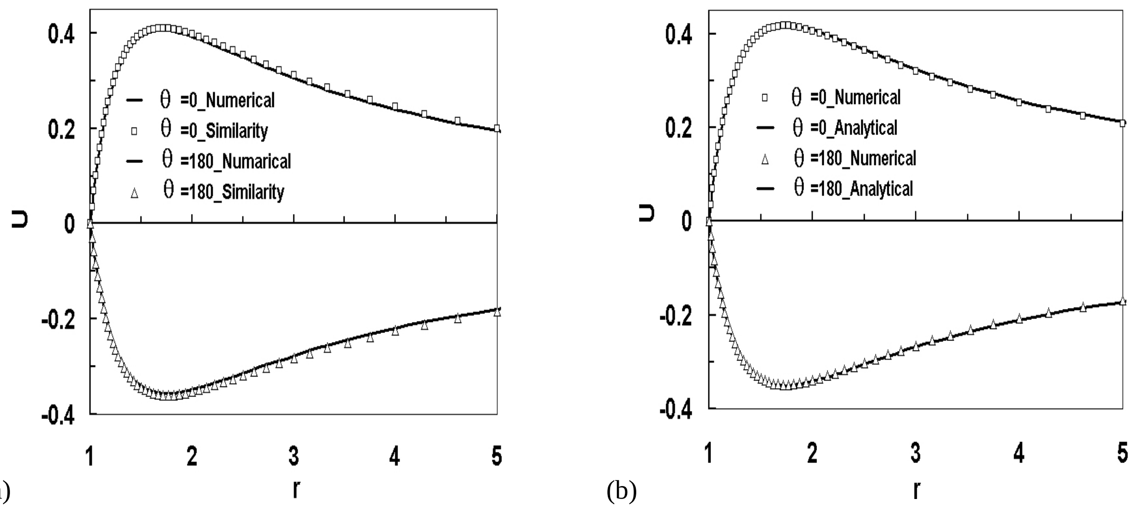

(a) (b)

Figure 7. Steady state radial velocity distribution at θ = 0 and 180 : (a) Ra = .1 , (b) Ra = .4

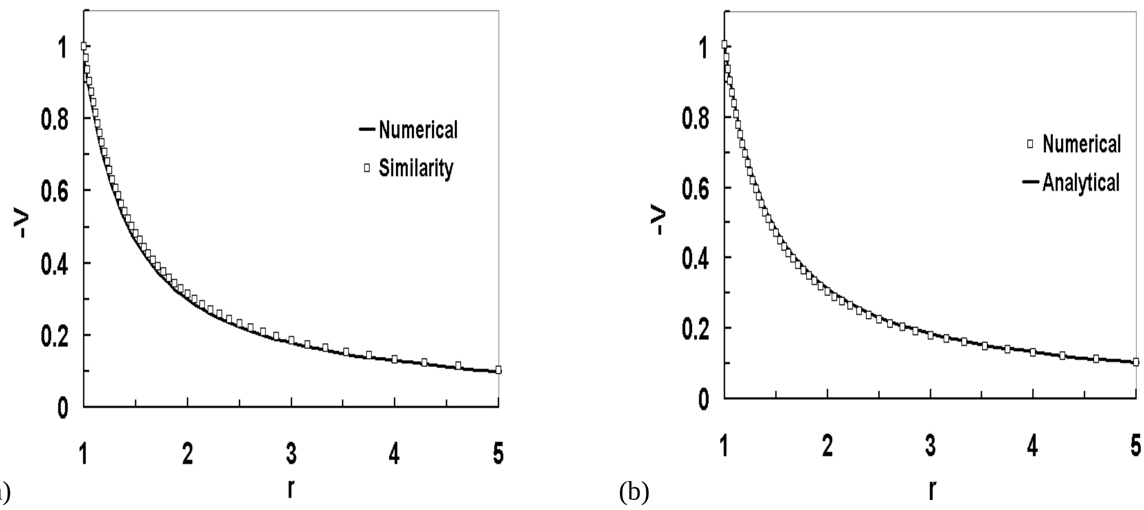

(a) (b)

Figure 8. Steady state tangential velocity distribution θ = 90 : Ra = .1 , (b) Ra = .4

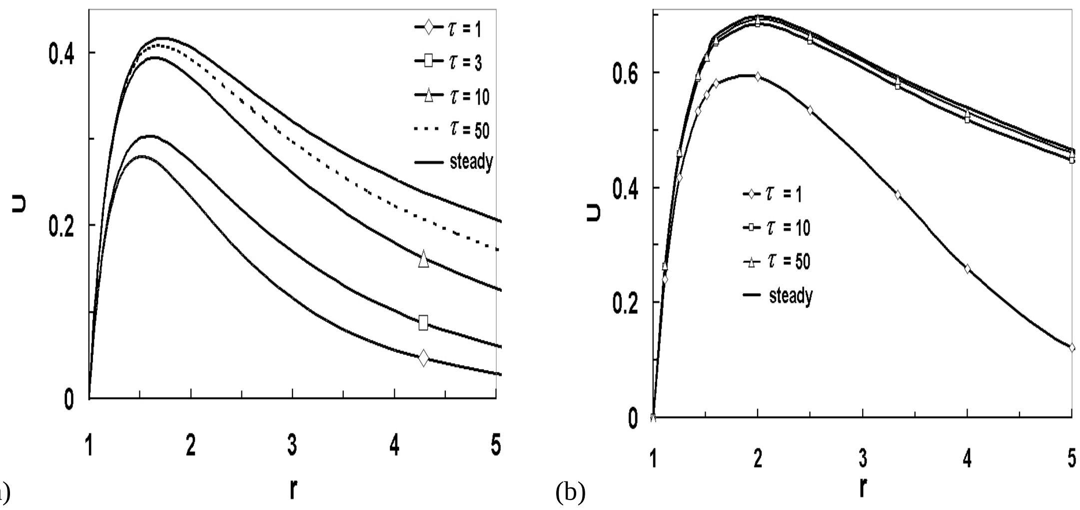

(a) (b)

Figure 9. Transient radial velocity distribution at θ = 0 in different times : (a) Ra = .4 , (b) Ra = 10

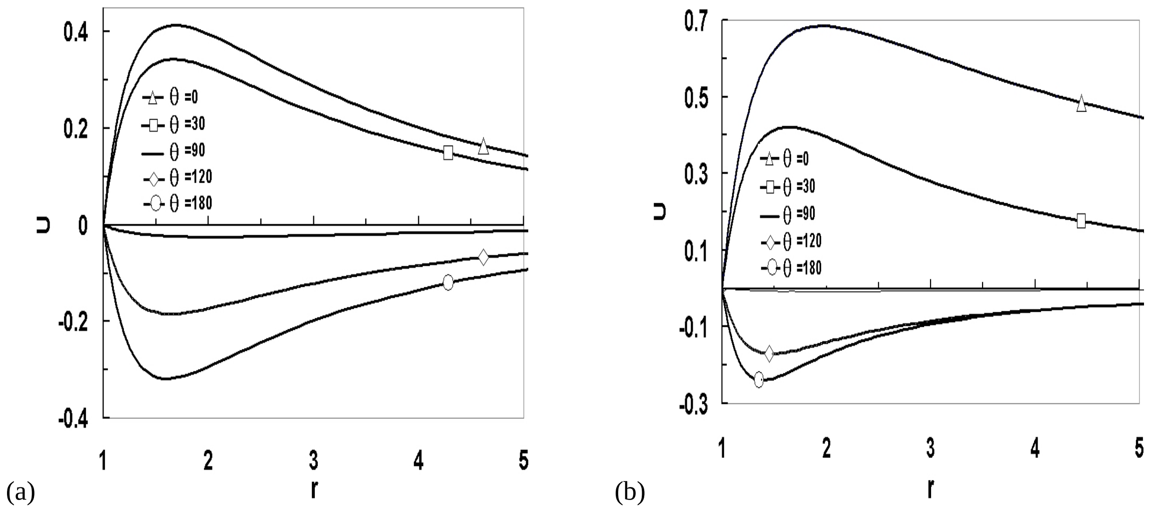

Figure 10. Transient radial velocity distribution at τ = 10 and different angles θ : (a) Ra = 1 , (b) Ra = 10

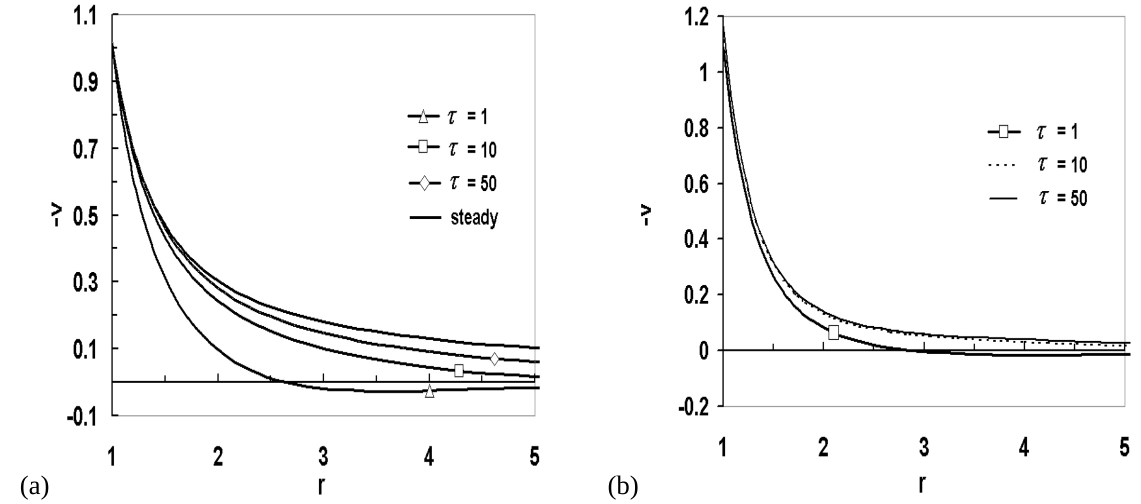

Figure 11. Transient tangential velocity distribution at θ = 90 in different times : (a) Ra = .4 , (b) Ra = 10

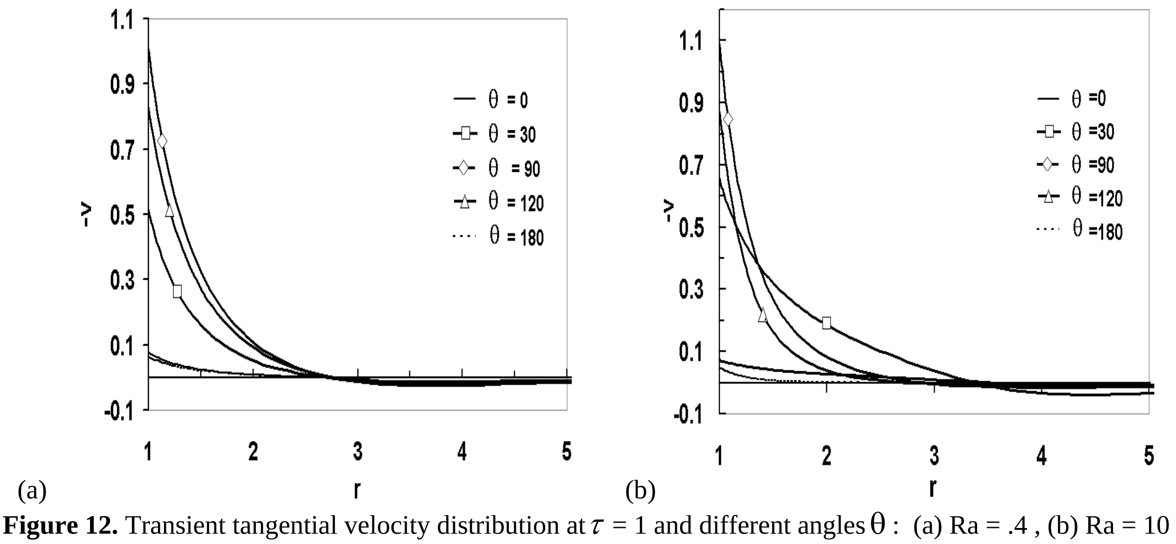

Figure 12. Transient tangential velocity distribution at τ = 1 and different angles θ : (a) Ra = .4 , (b) Ra = 10

values for other angles. All this is because of the way the streamlines vary, as mentioned before. Differentiating Equation (20) with respect to θ we have,

$$\frac{\partial Nu}{\partial \theta} = (-2a_1 + \frac{a_0}{4} Ra) \sin\theta \tag{59}$$

setting $\frac{\partial Nu}{\partial \theta} = 0$, for steady-state condition yields,

$$Ra)_{crit} = \frac{8a_1}{a_0}, \; Nu)_{crit} = a_0 + .4776 a_1 Ra)_{crit} \tag{60}$$

If for example, $a_0 = 1, a_1 = .1$, then $Ra)_{crit} = 0.8, \; and \; Nu)_{crit} = 1.0382$. This means that the local Nusselt number for this value of Ra number and in steady-state condition is independent of θ and this suggests that the buoyancy effects on the local Nusselt number at the top and bottom of the sphere cancel each other. Figures (13) and (14) show the variation of steady-state local Nusselt number with respect to θ for $Ra = 0.1, 0.4$ and for different functions of sphere surface temperature:

$$[T(s) = 2.2 - .015\theta - 0.14\theta^2 + 0.0289\theta^3,$$
$$T(s) = 1.0 - 0.1Exp(0.2\theta) - 0.1\theta^2 + 0.022\theta^3,$$
$$T(s) = 1.0 + 0.1\cos\theta\;]$$

As from these figures, there is a good agreement between results of analytical and numerical solutions. The main reason for differences are because in analytical solution all the surface temperature functions are approximated as a cosine function.

In Figure (15), the distribution of transient local Nusselt number in terms of θ for sphere surface temperature $T(s) = 1.0 + 0.1\cos\theta$ and for $Ra = 0.1$ at τ =3 and 10 are shown. Again we see that there is a very good agreement between numerical and analytical results and the differences are because in analytical solutions all the surface temperature functions are approximated as a cosine function.

Figure (16a) shows the value of steady-state local Nusselt number obtained analytically for $Ra = 0.1, 0.4, 0.8,$ and 1.0. It is clear that for lower Ra numbers like 0.1 and 0.4 variation of local Nusselt number is different than for greater Ra numbers like 0.8 and 1.0. For the former Ra numbers, the local Nusselt number decreases from its maximum value at $\theta = 0$ and reaches to its minimum value at $\theta = 180$. For Ra=0.8 variation of local Nusselt number is independent of θ and for $Ra = 1.0$ its variation changes completely so that at $\theta = 0$ its value is a minimum and at $\theta = 180$ is a maximum. Also it is evident from the figures that around $\theta = 0$ this quantity decreases with increasing Ra number. This is because both the convection and the surface temperature function affect the local Nusselt number. The function $T(s) = 1.0 + 0.1\cos\theta$ is such that temperature is a maximum at the top of the sphere ($\theta = 0$) and minimum value at the bottom ($\theta = 180$). Therefore, at initial moments and relative to constant temperature function $T(s) = 1.0$ the temperature difference between top surface and its near flow and its local Nusselt number is greater than that at the bottom of the sphere. But as time passes and as the effect of convection gets stronger, the fluid temperature around the sphere warms up and heat moves upwards. This is why at the same time that local Nusselt number decreases with respect to time the difference between Nusselt number at the top and bottom of the sphere decreases and at $Ra = 0.8$ becomes equal and that is why the local Nusselt number is independent of θ. As Ra increases, the convection effect is so large that at the initial stages the local Nusselt number at the top of the sphere is smaller than the bottom. In this state this quantity at $\theta = 0$ is a minimum and at $\theta = 180$ is a maximum. Also the thickness of thermal boundary layer at the top of the sphere and for large Ra numbers increases considerably. If we go back to Figures (5) and (6), we notice that because of the variation of surface temperature with respect to θ some of the isotherm lines initiate from the sphere surface. For small Ra numbers like 0.4, since the convection effects are weak and thermal conduction effects are stronger

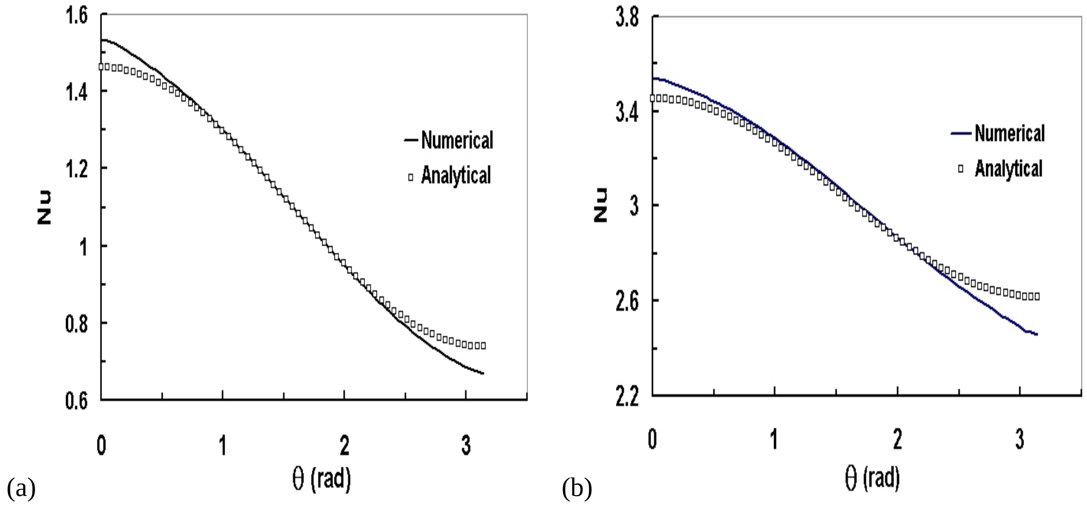

Figure 13. Steady-state distribution of local Nusselt number for numerical and analytical solutions and various functions of temperature on surface of sphere and for Ra = .1 , τ =1 (a) T(s) = 1-.1exp(.2 θ)-.1 θ^2 +.022 θ^3 (b) T(s) = 2.2-.015 θ -.14 θ^2 +.0289 θ^3

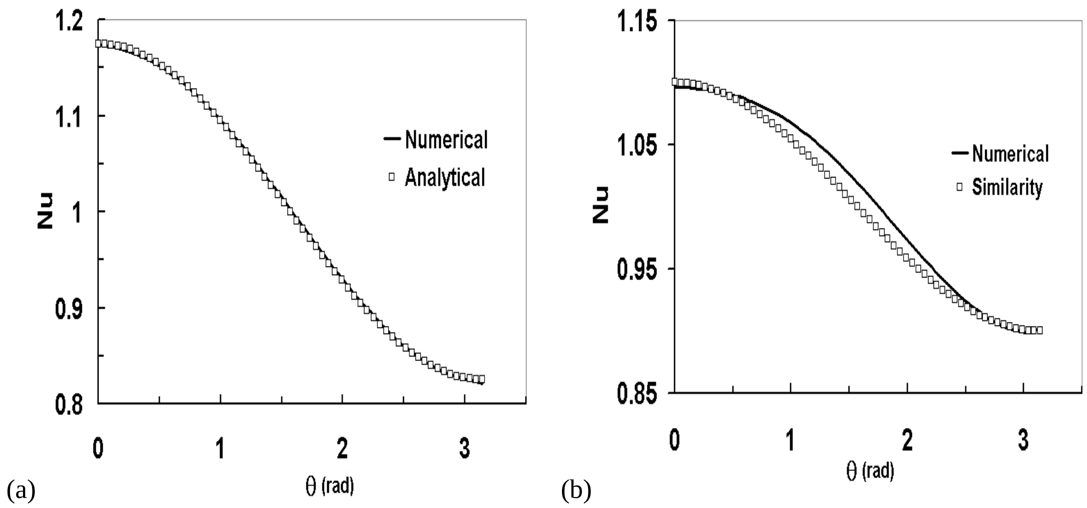

Figure 14. Steady state distribution of local Nusselt number for numerical and analytical solutions and T(s) = 1+.1 cos θ : (a) Ra = .1 (b) Ra = .4

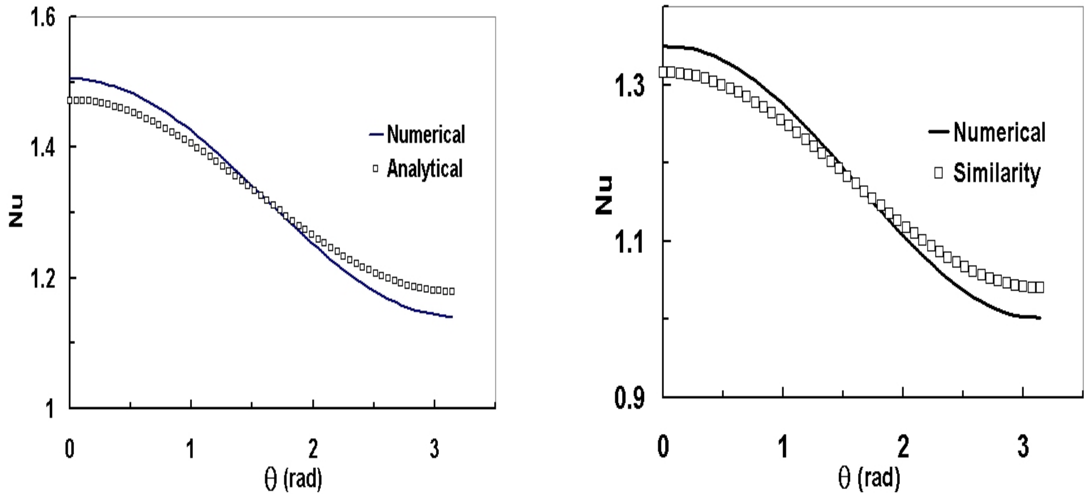

(a) (b)

Figure 15. Transient distribution of local Nusselt number for numerical and analytical solutions and Ra = .1 and T(s) = 1+.1 cos θ : (a) τ = 3 (b) τ = 10

and therefore the effects of surface temperature variation causes a greater local Nusselt number at the top relative to the bottom of the sphere. But for $Ra = 10.0$ the convection effects are dominant and a hot region is created at the top of the sphere and isotherm lines expand upwards. Also, the thermal boundary layer at the bottom of the sphere becomes very small and that is why the local Nusselt number at the bottom is greater than its corresponding value at the top.

Figure (16b) shows the transient local Nusselt number for $Ra = 0.1, 0.4, 1.0$ and 5.0 with respect to θ and at time $\tau =$ 3. We can clearly see, the changing direction of the variation of local Nusselt number between small Ra numbers such as $Ra = 0.1$ and 0.4 and higher Ra numbers such as Ra = 1.0 and 5.0. Also, for example, if we consider the curve lines for Ra = 0.1 and its intersection with other curves for other Ra numbers, we see that as Ra number increases, this intersection point moves to the left at the top of the sphere, $\theta = 0$. This is because of upward movement of the center of the vortex ring for higher Ra numbers and suggests that in this region the thickness of thermal boundary layer for higher Ra numbers becomes thinner.

In Figure (17), the results obtained for variable temperature case are compared with those for constant temperature case, for $Ra = 10$ and at $\tau =$ 1. It is observed that the magnitudes of radial velocities for variable temperature case and at θ = 0 are higher and at θ = 180 are smaller than those for constant temperature on surface of sphere. This is due to the fact that for variable temperature function $T(s) = 1.0 + 0.1\cos\theta$, the temperature difference in top and bottom of the surface of sphere is higher and smaller than those for constant temperature case, respectively. Because of this, at the top of the sphere and for temperature variable case, the activity of flow field is more and therefore the center of ring moves upward. It is seen that the magnitudes of tangential velocities at θ = 90 are almost equal for both cases. If we consider the variation of local Nusselt number, it is found that these values up to about θ = 110 are higher for variable temperature case in comparison with constant case and after this point become smaller. This is because that in top and bottom of the sphere temperature difference is higher and smaller than those for constant temperature case and this causes higher and smaller values for variable temperature case in top and bottom of the

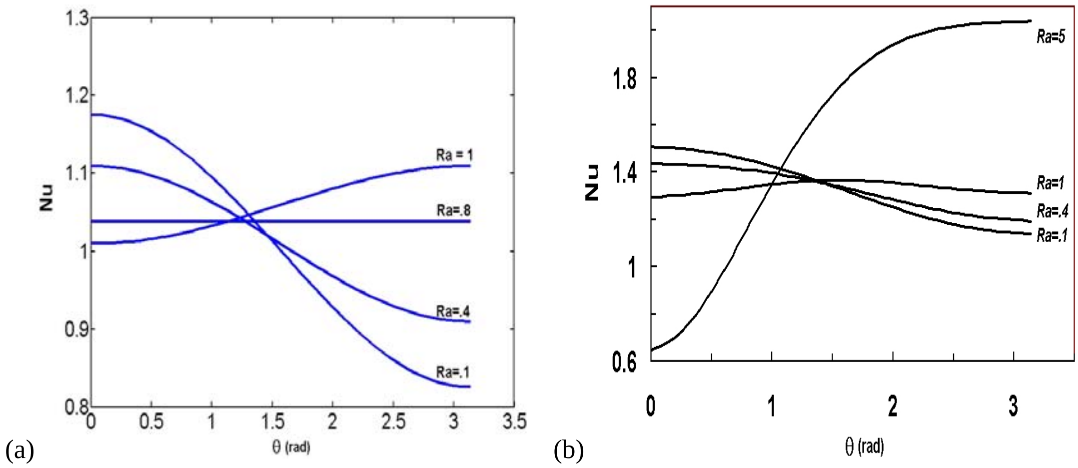

Figure 16. Distribution of local Nusselt number for different Ra number : (a) Analytical solutions and Steady state condition (b) Numerical solutions and at time $\tau = 3$

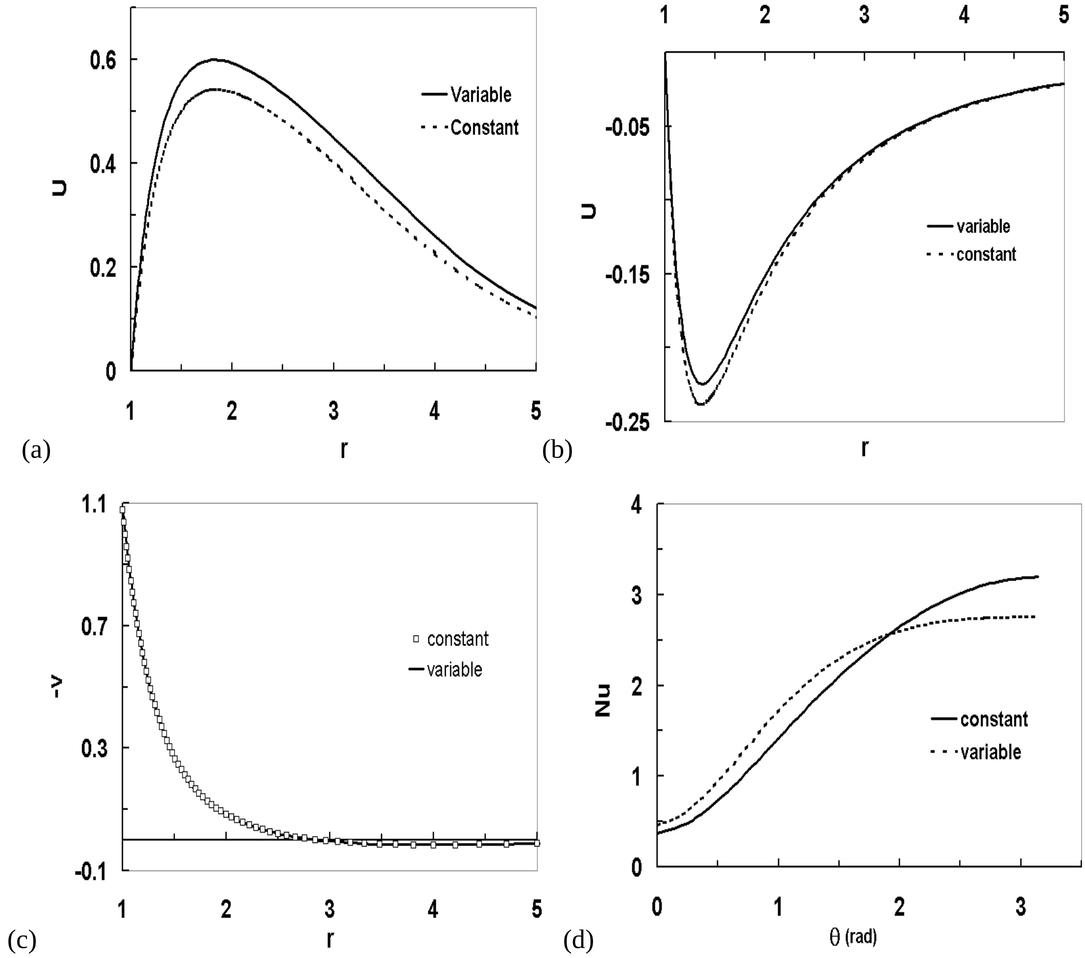

Figure 17. Comparison between results obtained for variable and constant temperature cases for Ra = 10 and time $\tau = 1$: (a) radial velocity at $\theta = 0$ (b) radial velocity $\theta = 180$ (c) tangential velocity at $\theta = 90$ (d) local Nusselt number

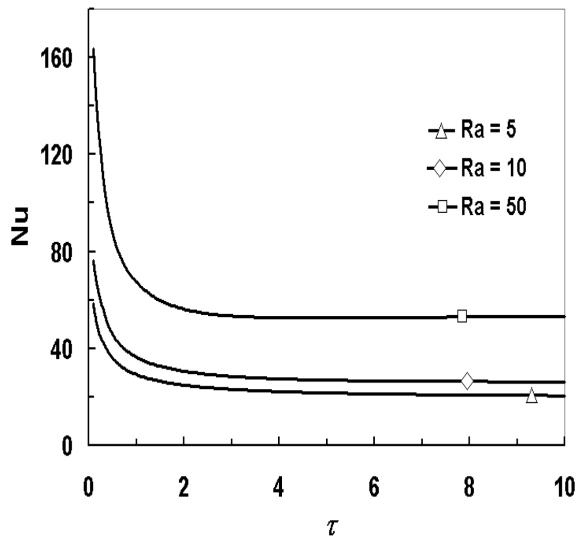

Figure 18. Average Nusselt number for different cases Of constant temperature and different Ra numbers

sphere, respectively. But at $\theta = 90^0$, even with surface temperature being equal for both cases, we observe that the Nusselt number is not the same and it is greater for variable surface temperature case. This is because, in variable temperature case the activity in top of the sphere becomes stronger and thus more hot particles are drawn toward the top and this causes, at this point, thickness of thermal layer to be smaller than the case of sphere with constant surface temperature.

Figure (18) shows the effect of Rayleigh number on average Nusselt number for different cases of constant temperature. As it is expected, the Nusselt number increases by increasing Rayleigh number.

6. CONCLUSIONS

Transient free convection heat transfer from a sphere with variable surface temperature in a porous medium has been studied for small an finite values of Ra numbers by numerical and analytical methods.

The results obtained by numerical method are in excellent agreement with those obtained by analytical method for small Ra numbers and with those presented in [9] for finite values of Ra numbers and constant temperature on surface of sphere. For high Ra numbers, such as $Ra = 10.0$ and 50, a buoyancy plume with a mushroom-shaped front is formed above the sphere.

A vortex ring is formed that moves up as Ra number increases. This causes higher values of radial velocities above the sphere and smaller values around its bottom for higher values of Ra number . For $T(s) = 1.0 + 0.1\cos\theta$, the magnitudes of steady-state local Nusselt number for $Ra = 0.1$ and 0.4 decrease from maximum value at θ = 0 to a minimum value at θ = 180. For $Ra = 0.8$, the local Nusselt Number is independent of θ and for higher Ra numbers, this variation of local Nusselt number is changed .

It is also seen that for sphere surface temperature, $T(s) = 1.0 + 0.1\cos\theta$, the values of local Nusselt number are higher than those for constant temperature case, up to approximately θ = 110 and after that, these values become smaller than those for constant temperature case. In this case the vortex ring moves upper and the radial velocities at $\theta = 0.0, 180^0$ become higher and smaller for variable temperature case, than those obtained for constant temperature case, respectively.

7. NOMENCLATURE

$erf(\eta)$	erf function
$F(r), G(\theta)$	functions
g	acceleration due to gravity
k	permeability of porous med.
n	integer
Nu	Nusselt number
$P_n(\cos\theta)$	Legender function
r	non-dim. Radial coord.
r_o	sphere radius
r', θ, ϕ	spherical coord. System
Ra	Rayleigh number
T	non-dim. Temperature
T_i	expansions of temp.
T_∞	surrounding temp.

T_w	surface temp.
u,v	non-dim. Velocity comp.
u'	radial velocity comp.
U_r	charact. Velocity
v'	transversal velocity comp.
X	new variable

Greek

α	constant
α_m	effective thermal diffusivity
β	coefficient of thermal exp.
ε	tolerance
η	variable
ρ	outer variable
τ	non-dim. Time
τ'	time
ψ	non-dim. Stream function
ψ'	stream function
ψ_i	expansions of stream function
υ	kinematic viscosity
∇	del operator

8. REFERENCES

1. K. Yamamoto, Natural Convection about a Heated Sphere in a Porous Medium, Journal of the Physics Society of Japan, 37, pp.1164-1166, 1974.
2. J. H. Merkin, Free Convection Boundary Layers On Axi-Symmetric and Tow-Dimensional Bodies Of Arbitrary Shape In Saturated Porous Medium, International Journal of Heat and Mass Transfer, **22**, pp.1461-1462, 1979.
3. P. Cheng, Natural Convection: Fundamentals and Applications. Hemisphere, Washington, DC, PP. 475, 1985.
4. A. Nakayama and H. Koyama, Free Convection Heat Transfer Over a Nonisothermal of arbitrary shape embedded in a fluid-saturated porous medium, Journal of Heat Transfer, 1987, 109, 125-130.
5. I. Pop and D. B. Ingham, Natural convection about a heated sphere in a porous medium, Proceeding of the Ninth International Heat Transfer Conference, 1990, vol. 2, pp. 567-572.
6. T. Sano and R. Okihara, Natural convection around a sphere immersed in a porous medium at small Rayleigh numbers, Fluid Dynamics Research, 1994, 13, 39-44.
7. T. Sano, Unstaedy Forced and Natural Convection Around A Sphere Immersed In A Porous Medium, Journal of Engineering Mathematics, 30:515-525, 1996.
8. H. D. Nguyen and S. Paik, Unsteady mixed convection from a sphere in water-saturated porous medium with variable surface temperature/heat flux, International Journal of Heat and mass transfer, 1994, **37**, 1783-1793.
9. B. Yan and I. Pop and D.B. Ingham, A numerical study of unsteady free convection from a sphere in a porous medium, International Journal of Heat and Mass Transfer, 1997 , Vol. 40, No. 4, pp. 893-903.
10. R. Nazar and I. Pop, On the mixed convection boundary-layer flow about a solid sphere with constant surface temperature, The Arabian J. for Science and Engr., vol. 27, No. 2c, Dec. 2002.
11. A. Kucaba-Pietal, Low-Reynolds-number flow of micropolar fluid between converging spheres, Int. j. of Engr. Science, vol. 38, issue 3, Feb. 2000.
12. R. S. Alassar, H. M. Badr, and H.A. Marromatis, Heat convection from a sphere in an oscillating free stream, Int. J. of Heat and Mass Transfer, vol. 42, issue 7, April 1999.
13. T. Sano and K. Makizono, Unsteady mixed convection around a sphere in a porous medium at low peclet numbers, Fluid Dynamics Research, 1998, 23, 45-61.
14. T. Sano, Unsteady flow past a sphere at low-Reynolds number, Journal of Fluid Mechanics, 1981, 112, 433-441.